Size and persistence length of molecular bottle-brushes by Monte Carlo simulations

Stefano Elli and Fabio Ganazzoli[a)]
Dipartimento di Chimica, Materiali e Ingegneria Chimica "G. Natta", Sez. Chimica, Politecnico di Milano, via L. Mancinelli 7, 20131 Milano, Italy

Edward G. Timoshenko[b)]
Theory and Computation Group, Centre for Synthesis and Chemical Biology, Conway Institute of Biomolecular and Biomedical Research, Department of Chemistry, University College Dublin, Belfield, Dublin 4, Ireland

Yuri A. Kuznetsov
Centre for High Performance Computing Applications, University College Dublin, Belfield, Dublin 4, Ireland

Ronan Connolly
Theory and Computation Group, Department of Chemistry, University College Dublin, Belfield, Dublin 4, Ireland

(Received 24 September 2003; accepted 6 January 2004)

Single-chain simulations of densely branched comb polymers, or ''molecular bottle-brushes'' with side-chains attached to every (or every second) backbone monomer, were carried out by off-lattice Monte Carlo technique. A coarse-grained model, described by hard spheres connected by harmonic springs, was employed. Backbone lengths of up to 100 units were considered, and compared with the corresponding linear chains. The backbone molecular size was investigated as a function of its length at fixed arm size, and as a function of the arm size at fixed backbone length. The apparent swelling exponents obtained by a power-law fit were found to be larger than those for the corresponding linear polymers, indicative of stiffening of the comb backbone. The probability distribution function for the backbone end-to-end distance was also investigated for different backbone lengths and arm sizes. Analysis of this function yielded the critical exponents, which revealed an increase in the swelling exponent consistent with values found from the molecular size. The apparent persistence length of the backbone was also determined, and was found to increase with increasing branching density. Finally, the static structure factors of the whole bottle-brushes and of their backbones are discussed, which provides another consistent estimate of the swelling exponents. [DOI: 10.1063/1.1651052]

I. INTRODUCTION

Molecular bottle-brushes are comb polymers with a high density of branches along the main chain (or backbone). Typically, such polymers are obtained by polymerization of an end-functionalized macromonomer,[1,2] and therefore they often carry a side chain per backbone monomer, so that no flexible spacer is present between adjacent branch points. If such a backbone carries sufficiently long arms, it displays an unusual rigidity characterized by an enhanced persistence length, despite the intrinsic flexibility of its chemical units.[1,3–7] This stiffness is related to the excluded-volume interactions among the side chains, and therefore it depends on their length. Because of this feature, amphiphilic molecular bottle-brushes carrying diblock copolymer side chains were used as templates for producing gold nanowires and clusters by loading the inner blocks with $HAuCl_4$ and subsequently reducing the salt to the metallic state.[5,8] Moreover, the enhanced backbone stiffness of these molecules produces two-dimensional local ordering on a surface,[4] and lyotropic main-chain liquid crystals.[3] A similar behavior was also found in related systems where end-functionalized oligomers strongly associate to linear polymers through hydrogen bonds.[9] The resulting system is akin to a bottle-brush where the side chains are held in place by interactions weaker than covalent bonds, and yet strong enough to induce mesomorphic behavior in the melt up to at least 80 °C.

Schmidt *et al.*[1,5,8] provided many experimental results on bottle-brushes by light-scattering and atomic force microscopy, and probed their use as templates for nanotechnologies. Some computer simulations were also carried out on these molecules, including both on-lattice[10,11] and off-lattice[6,12] methods. In particular, the MC simulations of ten Brinke *et al.*[12] focused on the possible lyotropic behavior of these systems, investigating the molecular aspect ratio, although only at a fixed backbone length. Theoretical analysis of this issue[13] has shown that the aspect ratio of bottle-brushes should increase with the arm length slightly faster than pro-

a)Author to whom correspondence should be addressed. Electronic mail: fabio.ganazzoli@polimi.it
b)Electronic mail: edward.timoshenko@ucd.ie. Web page: http://darkstar.ucd.ie

portionally, so that lyotropic behavior may be expected only asymptotically. Earlier, the influence of branching on the behavior of comb polymers had been investigated by Birshtein *et al.*,[14] through scaling methods assuming a roughly constant aspect ratio. We point out here that there is a substantial disagreement among the experimental, simulation, and theoretical studies concerning, for instance, the swelling exponent relating the molecular size to the backbone length. This exponent was theoretically predicted to be the same as in linear chains,[13,14] in keeping with some computer simulations,[11] but in clear disagreement with other ones[10] and with experimental results.[1] A similar disagreement was also found for the swelling exponent relating the arms size to their length.[5,10,13]

From a theoretical and computational viewpoint, molecular bottle-brushes comprise a subset of branched polymers, for which generic techniques were developed by our Milan and Dublin groups, irrespective of the connectivity of the macromolecular architecture.[15–17] In the past, we successfully applied these techniques to studies of stars and dendrimers, both homopolymers and copolymers.[15,16,18] Given that there are still open issues and some controversy about the conformational behavior of molecular bottle-brushes, we carried out an independent study of these systems. In particular, in addition to a new estimate of the swelling exponents and of the backbone stiffness, we investigated in detail both more advanced statistical observables, such as the probability distribution functions (PDF) and the critical exponents associated with them, and the static structure factors of the whole molecule or of its backbone, that may be directly compared with appropriately designed experiments after suitable labeling. To the best of our knowledge, a systematic study of these quantities has not yet been carried out so far.

A well-tested approach based on Monte Carlo simulations in continuous space is applied here to study flexible homopolymer bottle-brushes in a good (athermal) solvent. As we are interested in the generic features of bottle-brushes, we use a coarse-grained bead-and-spring model, assuming no intrinsic rigidity for the backbone or the side chains. The inter-bead potential is simply described through hard-sphere interactions, so that we indeed have an athermal system, equivalent to a self-avoiding walk with the connectivity constraints. In the next section, we briefly summarize the model and the simulation methodology, and define the relevant observables and the procedure used to estimate their standard errors. Afterwards, we discuss our results in terms of (i) the molecular size and its dependence on the backbone and arm length; (ii) the probability distribution function of the backbone end-to-end-distance and the relevant critical exponents; (iii) the apparent persistence length of the backbone and the molecular aspect ratio; (iv) the static structure factors of the whole molecule and of the backbone.

II. SIMULATION METHOD

We adopt a bead-and-spring model with a hard-sphere interaction potential to describe excluded-volume interactions (athermal solvent). The system Hamiltonian is given by

$$H=\frac{k_BT}{2\ell^2}\sum_{i\sim j} r_{ij}^2+\frac{1}{2}\sum_{i\neq j} V(r_{ij}), \tag{1}$$

where $r_{ij}=|\mathbf{X}_i-\mathbf{X}_j|$, $\mathbf{X}_i$ being the vector position of the ith bead. In Eq. (1), the first sum accounts for the harmonic springs between connected beads, indicated by $i\sim j$, and the second one for the pairwise interaction potential. For a hard-sphere potential, $V(r)$ is given by

$$V(r)=\begin{cases}+\infty & \text{if } r<d,\\ 0 & \text{if } r>d,\end{cases} \tag{2}$$

where d is the sphere diameter. With the definition of the spring constant in Eq. (1), the mean-square distance between connected beads in a random walk is $\langle r_{i,i+1}^2\rangle=3\ell^2$. In the following, we use the reduced units $k_BT=1$ and $\ell=1$, and take $d=\ell$ as a convenient choice.

We consider comb polymers with N_b backbone beads and f arms, each comprising N_a beads, evenly distributed along the backbone. It is useful to define the branching density $m=f/N_b$, so that the total number of beads is $N=N_b+f\cdot N_a=N_b(1+m\cdot N_a)$. Here, we study highly branched comb polymers with $m=0.5$ and 1 (neglecting the end beads), indicated for brevity as low- and high-density (or LD and HD) bottle-brushes. Note that for $m=0$ and for $N_a=0$ we obtain a linear chain with the same length as the corresponding comb backbone.

We employ the Monte Carlo method in continuous space using the standard Metropolis algorithm as described in detail in previous papers.[15] The procedure involves random local moves of a randomly selected bead with a minimum displacement of 0.05 (in ℓ units) adjusted to achieve an acceptance ratio of 0.5, which helps to avoid nonergodicity issues in the phase-space sampling. We carried out long simulation runs of Q independent samples, collecting a large number t of almost independent configurations after equilibration to calculate the statistical averages. The t configurations were separated by a large number of sweeps ($\sim N^2$, a sweep corresponding to N attempted moves), but in principle could still display residual correlations affecting the estimated standard errors. Let us denote as A_i^j, $i=1,2,...,t$, $j=1,2,...,Q$ the value of the generic observable A in the ith configuration of the jth sample. If all the Qt values of A_i^j were uncorrelated, then the average value of A would be

$$\langle A\rangle=\frac{1}{Qt}\sum_{j=1}^{Q}\sum_{i=1}^{t} A_i^j,$$

the dispersion of its distribution

$$\sigma^2(A)=\frac{1}{Qt}\sum_{j=1}^{Q}\sum_{i=1}^{t}(A_i^j-\langle A\rangle)^2$$

and the standard error on $\langle A\rangle$ $\delta A=\sqrt{\sigma^2(A)/Qt}$. However, if there is any correlation between the t configurations of the Q independent samples, then there is a statistical inefficiency $s>1$ such that actually $\delta A=\sqrt{\sigma^2(A)\cdot s/Qt}$. In order to estimate s, we group the t configurations of a given run in l_b blocks, each comprising τ_b configurations ($t=l_b\cdot\tau_b$) and calculate the average

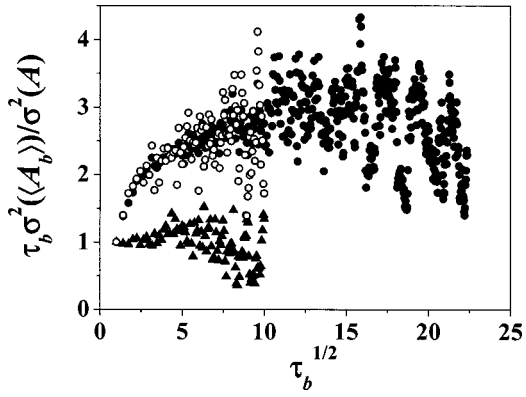

FIG. 1. An example of the estimate of the statistical inefficiency s for three LD bottle-brushes with $N_a=5$ beads per arm. The three cases correspond to $N_b=10$ sampled for $t=1000$ configurations (filled triangles), and $N_b=70$ sampled for a total of $t=1000$ and 5000 configurations (empty and filled circles), the number of blocks being in all cases $l_b \geqslant 10$. Here the observable A is the molecular radius of gyration, while τ_b is the number of configurations sampled in a block (see text).

$$\langle A \rangle_b = \frac{1}{\tau_b} \sum_{i=1}^{\tau_b} A_i$$

and variance

$$\sigma^2(\langle A \rangle_b) = \frac{1}{l_b} \sum_{b=1}^{l_b} (\langle A \rangle_b - \langle A \rangle)^2.$$

Upon increasing the block length, we expect the correlation within each block to decrease so that $\sigma^2(\langle A \rangle_b) \sim 1/\tau_b$ for large τ_b due to the central limit theorem. Therefore, we can estimate[19] s from the relationship $s = \lim_{\tau_b \to +\infty} [\tau_b \sigma^2(\langle A \rangle_b)/\sigma^2(A)]$. An example of such estimate is reported in Fig. 1, where A is the molecular radius of gyration. All standard errors in the following were corrected for statistical inefficiency according to this procedure.

The average quantities characterizing the molecular size are the mean-square interbead distances, $\langle r_{ij}^2 \rangle$, and the backbone mean-square end-to-end distance, $\langle R_b^2 \rangle$, and radius of gyration, $\langle S_b^2 \rangle$, the latter being given by the mean-square distance of the backbone beads from their center of mass,

$$\langle S_b^2 \rangle = \frac{1}{2N_b^2} \sum_{i,j=1}^{N_b} \langle r_{ij}^2 \rangle. \tag{3}$$

Analogous expressions can be used to characterize the arms, with an a subscript, or the whole molecule, with no subscript.

Another important quantity, not easily accessible experimentally, is the probability distribution function (or PDF) of the distance between the generic bead pair i,j, which is obtained through the expression

$$g_{ij}(r) = \langle \delta(\mathbf{r}_{ij} - \mathbf{r}) \rangle = \frac{1}{4\pi r^2} \langle \delta(|\mathbf{r}_{ij}| - r) \rangle. \tag{4}$$

In the following, we focus on the PDF for the backbone end-to-end distance, where $r_{ij} = R_b$.

The chain stiffness is characterized through the persistence length along the backbone. Among the possible definitions of persistence length, we adopt the following one, in terms of the projection of the backbone end-to-end vector $\mathbf{R}_b$ on the generic kth spring[20]

$$l_{\text{pers}}^{(k)} = \left\langle \frac{\mathbf{r}_{k,k+1}}{|\mathbf{r}_{k,k+1}|} \cdot \mathbf{R}_b \right\rangle. \tag{5}$$

In general, $l_{\text{pers}}^{(k)}$ may depend on the spring location within the main chain.

Finally, the static structure factor of the backbone is obtained from the expression

$$\begin{aligned} S_b(q) &= \frac{1}{N_b^2} \sum_{i,j=1}^{N_b} \tilde{g}(|\mathbf{q}|), \\ \tilde{g}(\mathbf{q}) &= \langle \exp[i\mathbf{q} \cdot (\mathbf{X}_i - \mathbf{X}_j)] \rangle \\ &= \frac{1}{2\pi^2} \int_0^\infty r^2 g_{ij}(r) \frac{\sin(qr)}{qr} dr, \end{aligned} \tag{6}$$

q being the scattering vector [$q = |\mathbf{q}| = 4\pi \sin(\theta/2)/\lambda$, θ being the scattering angle and λ the radiation wavelength], while the double sum is performed over the i,j bead pairs of the backbone. An analogous expression can be written for the whole molecule dropping the b subscripts.

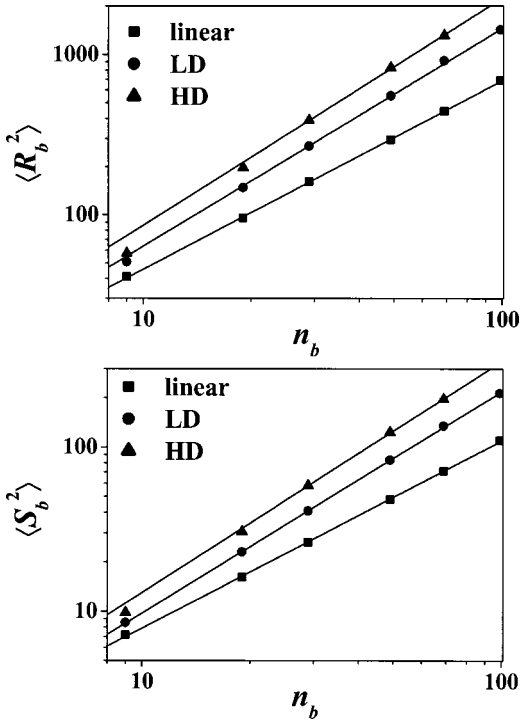

FIG. 2. The mean-square backbone end-to-end distance $\langle R_b^2 \rangle$ and radius of gyration $\langle S_b^2 \rangle$ plotted as a function of the backbone length n_b for linear chains (squares) and LD and HD bottle-brushes (circles and triangles) with $N_a=5$ beads per arm. The solid lines are the power-law fitting curves according to Eq. (7), the best-fit parameters being in Table I. In all cases, the error bars are smaller than the symbol size.

III. RESULTS AND DISCUSSION

A. The molecular size

The backbone mean-square end-to-end distance $\langle R_b^2 \rangle$ and radius of gyration $\langle S_b^2 \rangle$ are shown in Fig. 2 as a function

TABLE I. The fitting parameters of Eqs. (7) and (8) for linear chains and LD and HD bottle-brushes with $N_a=5$ beads per arm. The standard errors on the last significant digit(s) are reported in parentheses.

	$\langle R_b^2\rangle$		$\langle S_b^2\rangle$		$\langle r_{ij}^2\rangle$	
	a_R	ν_R	a_S	ν_S	a_{ij}	ν_{ij}
Linear	3.04(6)	0.588(2)	0.570(6)	0.570(1)	3.73(1)	0.5770(5)
LD	2.80(5)	0.678(2)	0.438(8)	0.674(2)	3.823(3)	0.6639(1)
HD	3.2(4)	0.707(17)	0.51(5)	0.703(11)	4.28(3)	0.707(1)

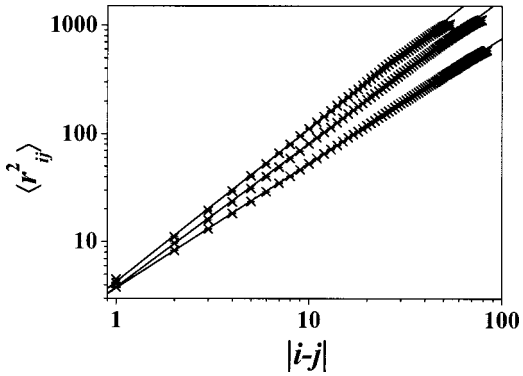

FIG. 3. The mean-square distance between backbone beads $\langle r_{ij}^2\rangle$ plotted as a function of their topological separation $|i-j|$ for the linear chain (lower curve) and LD and HD bottle-brushes (central and upper curve, respectively) with $N_a=5$ beads per arm. The backbone comprises $N_b=100$ beads and the starting bead is $i=20$ ($N_b=70$ and $i=15$ in HD bottle-brush). The straight lines are the fits to the power law of Eq. (8) neglecting the terminal 20 beads (15 in HD bottle-brush) to avoid end effects (visible as a slight downturn at large $|i-j|$ due to the larger swelling of the central portions). The best-fit parameters are in Table I. In all cases, the error bars are smaller than the symbol size.

of the backbone length $n_b=N_b-1$ for the LD and HD bottle-brushes at a fixed arm length, $N_a=5$, in comparison with linear chains. It can be seen that bottle-brushes have a much larger size than linear chains of the same backbone length, the more so the larger is the branching density due to the repulsive interactions among the arms that force the backbone to assume a slender shape. Of course, this effect becomes stronger both with a larger arm density, and with longer arms due to their larger excluded volume.

The data points in the figures cannot be fitted by theoretical equations valid for stiff chains such as the wormlike model. Therefore, they were simply fitted with the power law

$$\langle X^2\rangle = a_x \cdot n_b^{2\nu_x}, \tag{7}$$

where X is either R_b or S_b, and ν_x the corresponding swelling exponent. The best-fit values of a_x and ν_x (solid lines in Fig. 2) are reported in Table I with their standard errors.

For linear chains, ν_R is equal to the current best theoretical and simulation results of the Flory exponent,[17,21] while ν_S is slightly smaller because it reaches its asymptotic value more slowly. Therefore, the values in Table I may still be in the crossover region. In fact, for finite chains the mean-square radius of gyration can still be affected by topologically close bead pairs not yet in the asymptotic regime. On the other hand, bottle-brushes show much larger exponents (see Table I) even with $N_a=5$ beads per arm only, while for shorter arms the swelling exponents are closer to the linear-chain value. It may also be noted that at short backbone length both $\langle R_b^2\rangle$ and $\langle S_b^2\rangle$ are smaller than the value predicted by Eq. (7): this feature, particularly evident in the HD bottle-brush, reflects a crossover towards a compact molecular topology somewhat reminiscent of star polymers.

Another interesting quantity is the plot of the mean-square distances among the beads $\langle r_{ij}^2\rangle$ as a function of their topological separation $|i-j|$. Considering the backbone beads, these plots provide a check of the swelling exponents, because in analogy with Eq. (7) we expect a power law relationship

$$\langle r_{ij}^2\rangle = a_{ij} \cdot |i-j|^{2\nu_{ij}} \tag{8}$$

with ν_{ij} equal to ν_R and ν_S in the long-chain limit. A typical result for linear chains and for LD and HD bottle-brushes with an arm length of $N_a=5$, is shown in Fig. 3, while the fitting results (solid lines) are reported in Table I. In all cases the exponents ν_{ij} are consistent with those of the whole backbone. In particular, for linear chains ν_{ij} lies between ν_S and ν_R, thus confirming that ν_S reaches the asymptotic value more slowly. Moreover, these results produce again the large value of the swelling exponent of bottle-brushes.

A recent lattice simulation study[11] appears to be in conflict with our results. In fact, for similar backbone lengths and branching density, a swelling exponent $\nu_R=0.588(65)$ was reported, equal to the Flory exponent of linear chains (the value in parentheses is the standard error on the last significant digits). While lattice artefacts, which are known to be difficult to deal with for branched systems, cannot be ruled out, the reported exponent is quite surprising in view of our results, even in the presence of the large error margin. On the other hand, other lattice simulations using the bond fluctuation model yielded different results consistent with ours.[10] In particular, for HD bottle-brushes ν_S was found to increase with the arm length from 0.60(1) for $N_a=0$ (linear chain) up to 0.97(5) for $N_a=64$, with a value of 0.69(1) for $N_a=4$ that nicely agrees with our value in Table I.

Interestingly, our swelling exponents do reasonably agree with the experimental results of Schmidt *et al.*[1] at a constant arm length. These results were fitted with the wormlike-chain model, even though some discrepancies were apparent at ''low'' molar masses. However, we can analyze the same data in terms of a power-law relationship in the ''high''-molar-mass region either graphically, or by fitting the wormlike curve employing Schmidt's parameters. Notably, we obtain an apparent exponent that increases from 0.60 to 0.63 up to 0.68 for arms with 28, 38, and 54 monomers, in fair agreement with our results.

As for the arm length, the mean-square end-to-end distance $\langle R_a^2\rangle$ can also be expressed through a power-law dependence on the number of bonds n_a,

$$\langle R_a^2\rangle = a_{\mathrm{arm}} \cdot n_a^{2\nu_{\mathrm{arm}}} \tag{9}$$

in analogy to what done for the backbone. We first point out that most arms display a uniform size within a given bottle-brush independent of their location along the main chain, apart from those close to the free ends, and independent also

of the backbone length, suggesting that the interarm repulsion is essentially local. The best-fit parameters in Eq. (9) for an LD bottle-brush with $N_b=20$ are $a_{\rm arm}=3.24(4)$ and $\nu_{\rm arm}=0.608(3)$, slightly but significantly larger than the linear-chain value (see Table I). The increase of $\nu_{\rm arm}$ above 0.588(2) due to the interarm repulsions is much less than that found for the backbone, but it agrees with the value 0.60(1) previously obtained with the bond fluctuation model.[10] On the other hand, this exponent is not as large as the value of 0.682 recently found by other simulations,[6] or the theoretically predicted[13] one of 0.75.

It should be stressed that our swelling exponents for the bottle-brush backbone are apparent ones, being slightly dependent on its length. This feature is particularly evident for the HD bottle-brush at small n_b (see Fig. 2), where the molecules bear some similarity to star polymers due to their short backbone length. Thus, the exponents may change somewhat in the asymptotic limit $N_b\to\infty$. In fact, general theoretical arguments suggest that the ν exponent of linear chains and of comb polymers with finite side chains should eventually coincide. These arguments rely on the observation that for a fixed arm length the comb diameter, conveniently defined as $2\langle R_a^2\rangle^{1/2}$, is independent of the backbone length,[10] as pointed out after Eq. (9). Therefore the ratio between the backbone contour length and the diameter diverges for $N_b\to\infty$, making the molecule akin to a linear chain. Accordingly, the influence of side chains can be described purely via effectively renormalizing the persistence length of an equivalent linear chain. Clearly then, a semiflexible chain would become totally flexible if the number of links tends to infinity but the persistence length remains finite, and ν would eventually be 0.5882 for both topologies. A rigorous proof of this argument could only be obtained by an accurate renormalization group study, but this task is not easy, given that one must somehow retain the finite arm length. Moreover, it is possible that the effective semiflexible linear chain idea may be somewhat flawed due to nonlocal effects mediated by the arm volume interactions. On the other hand, our results suggest that in bottle-brushes with a very large branching density such limit might only be reached for huge backbone lengths, well outside the experimentally accessible range. Therefore, while the above limit is of great interest academically, it may be irrelevant in practice.

We now consider the dependence of the overall molecular size on the arm length N_a for a fixed backbone length N_b. We report again results obtained for the mean-square end-to-end distance of the backbone, $\langle R_b^2\rangle$, using short LD bottle-brushes with $N_b=10$ and 20 beads. The results shown in Fig. 4, normalized by the corresponding linear-chain value $\langle R_b^2\rangle_{\rm lin}$, indicate that the interarm repulsions significantly increase the molecular size with increasing N_a, up to an asymptotic constant value, with a corresponding backbone stiffening. The data points can be fitted by the saturation curve, $\langle R_b^2\rangle/\langle R_b^2\rangle_{\rm lin}=1+A[1-\exp(-N_a/B)]$. This expression correctly reduces to unity for $N_a=0$, while A gives the relative increase of $\langle R_b^2\rangle$ over $\langle R_b^2\rangle_{\rm lin}$ in the asymptotic limit. The fitting parameters A and B, reported in the figure caption, depend on the backbone length and on the branching density, but we cannot extract general relationships apart from saying that they increase with N_b.

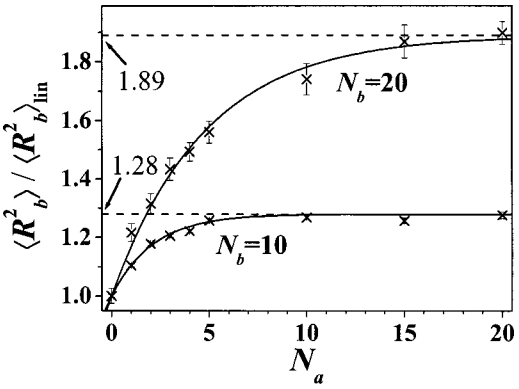

FIG. 4. The normalized mean-square backbone end-to-end distance of two LD bottle-brushes with different backbone length plotted as a function of the arm length N_a. The normalization factor $\langle R_b^2\rangle_{\rm lin}$ is the mean-square end-to-end distance of the corresponding linear chain. The solid lines are the best-fit saturation curves $\langle R_b^2\rangle/\langle R_b^2\rangle_{\rm lin}=1+A[1-\exp(-N_a/B)]$ with fitted values $A=0.277(6)$ and $B=2.1(1)$ for the shorter, and $A=0.89(3)$ and $B=4.7(4)$ for the longer comb. The horizontal asymptotes are shown with dashed lines.

The saturation curves of Fig. 4 are certainly affected by the short backbone length, which prevents an unbound increase in $\langle R_b^2\rangle$ and produces an almost starlike behavior of the molecules at large N_a. However, though large, the present values still indicate a coiled backbone conformation with some apparent stiffening. While the backbone behaves as a coil at scales beyond the persistence length, it does not compare to a semiflexible linear chain of the same persistence length, as said before. For instance, conformations of the latter would never exhibit any sharp turns, which would be energetically rather unfavorable, whereas our Hamiltonian does not really penalize the backbone for doing a few sharp turns. Thus, a semiflexible linear chain is not fully equivalent to the comb backbone.

B. The probability distribution functions

The probability distribution function (PDF) of the distances among the bead pairs, $g_{ij}(r)$, was defined in Eq. (4). For convenience, we report it in the reduced dimensionless form

$$\hat{g}_{ij}(\hat{r})=\langle r_{ij}^2\rangle^{3/2}g_{ij}(r),\quad \hat{r}=r/\langle r_{ij}^2\rangle^{1/2}. \tag{10}$$

In this way, the reduced PDF satisfies the double normalization conditions[17]

$$\int_0^{+\infty}d\hat{r}\,\hat{r}^2\hat{g}_{ij}(\hat{r})=\int_0^{+\infty}d\hat{r}\,\hat{r}^4\hat{g}_{ij}(\hat{r})=\frac{1}{4\pi}. \tag{11}$$

We focus here on the reduced PDF of the end-to-end distance, indicated as $\hat{g}_R(\hat{r})$. This function is shown in Fig. 5 for two linear chains and two LD bottle-brushes of different backbone length. In keeping with previous theoretical and simulation results,[17,22–24] we fitted the data points with the function

$$\hat{g}_R(\hat{r})=A_0\cdot\hat{r}^{\vartheta_0}\exp(-B_0\cdot\hat{r}^{\delta_0}). \tag{12}$$

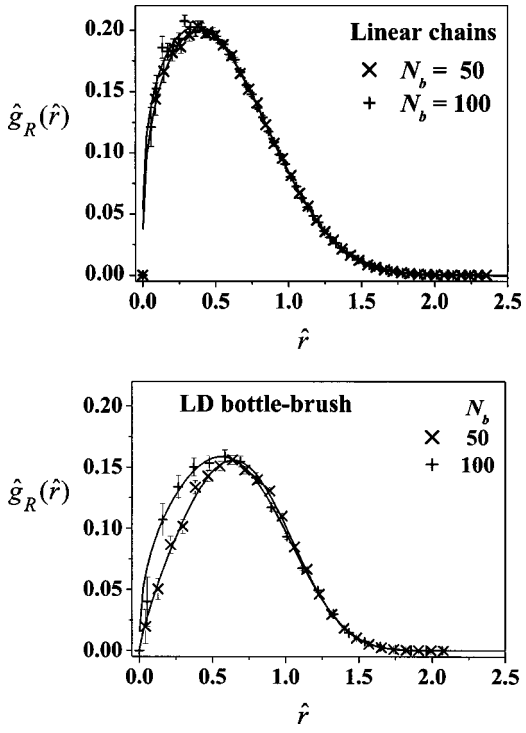

FIG. 5. The probability distribution function for the end-to-end distance R_b of a linear chain with $N_b=50$ and 100 beads and for an LD bottle-brush with two backbone lengths ($N_b=50$ and 100 beads) and an arm length of $N_a=5$ beads. The data were obtained with 1.5×10^5 and 3.0×10^5 independent samples for the linear chain, and with 4.0×10^4 and 2.0×10^4 independent samples for the LD bottle-brushes. The solid lines are the fitting curves obtained with Eq. (12) with the parameters reported in Table II.

In principle, $\hat{g}_R(\hat{r})$ is expected to follow a simple power-law dependence[23] at small $\hat{r}$ [$\hat{g}_R(\hat{r})\propto\hat{r}^{\vartheta_0}$] reflecting the correlation hole at the origin due to the self-avoiding condition, and a power-law times a stretched exponential [$\hat{g}_R(\hat{r})\propto\hat{r}^{\vartheta_0}\cdot\exp(-B_0\cdot\hat{r}^{\delta_0})$] at large $\hat{r}$, the ϑ_0 exponent being somewhat different in the two limits. However, in practice the single Eq. (12) provides an excellent picture of the overall behavior of $\hat{g}_R(\hat{r})$.[17,22] Here the 0 subscript is meant to indicate the backbone end-to-end distance, following des Cloizeaux's notation,[24] while 1 and 2 subscripts are used to indicate the end-to-center and center-to-center distances. Due to the normalization conditions, the constants A_0 and B_0 have known expressions, but are treated here as fitting parameters just as ϑ_0 and δ_0 for simplicity.

For linear chains, δ_0 turns out to be independent of the backbone length (see Table II), and takes the average value of 2.42(2). Moreover, we checked that within the statistical accuracy, it is also equal to δ_1 (end-to-center beads) and δ_2 (center-to-center beads), in keeping with theoretical predictions.[25] Using for δ the relationship

$$\delta=(1-\nu)^{-1} \tag{13}$$

we obtain a new estimate for the Flory exponent, $\nu=0.587(4)$, in excellent agreement with what obtained by the power-law fit of Eq. (7) to the mean-square end-to-end distance (see Table I). As for ϑ_0, it weakly depends on the backbone length and cannot be unambiguously extrapolated to an asymptotic value. However, the value for the long linear chain with 100 beads is in good agreement with the theoretical value 0.271(2).[21] From ϑ_0 (see Table II), we can estimate the critical exponent γ. Two relationships were obtained for flexible linear chains,[23,24]

$$\vartheta_0=\frac{\gamma_A-1}{\nu}, \tag{14'}$$

$$\vartheta_0=\frac{3\nu-\gamma_B-1/2}{1-\nu}. \tag{14''}$$

The former expression is the short-distance version, relevant to describe the contact probability density, whereas the latter one applies to the long-distance tail of the PDF, which is obtained more accurately by our simulations. In turn, γ yields the number of self-avoiding walks Z_n for a chain with n segments ($n\to\infty$),

$$Z_n\sim Z n^{\gamma-1}\mu^n \quad (Z,\mu=\text{const}). \tag{15}$$

Using the fitted values of ϑ_0 and ν, given by Eq. (13), we obtain two different values of γ via Eqs. (14′) and (14″), with γ_A weakly decreasing and γ_B increasing with chain length. However, for the largest chain, the values match within the standard error, close to the theoretical value[21] $\gamma=1.160(2)$. Additionally, for linear chains our values of ϑ_1 and ϑ_2 (end-to-center and center-to-center beads) are 0.47(1) and 0.84(2), again in close agreement with previous simulation[17] and theoretical results.[24,26]

The PDF for the backbone end-to-end distance of LD bottle-brushes display a maximum at larger $\hat{r}$ than linear chains, and become broader, but their overall shape is qualitatively similar, and is again well reproduced by Eq. (12) (solid curves in Fig. 5). The best-fit parameters reported in Table II show that both δ_0 and ϑ_0 are larger than in linear chains. Assuming that Eqs. (13) and (14) also apply to the comb backbone, we can derive the apparent critical exponents ν and γ shown in Fig. 6. The swelling exponent ν, much larger than for linear chains, is fully consistent with the value previously found for the power-law dependence of the backbone size. Again, this exponent weakly depends on the backbone length, and when plotted versus N_b^{-1} [see Fig. 6(a)] it can be linearly extrapolated for $N_b^{-1}\to0$ to an asymptotic value of 0.706(7), even larger than that found for finite chains (see Table I). From ϑ_0 and Eqs. (14) we derive two values of γ that show a different dependence on N_b [see Fig. 6(b)], and do not converge to a common value. Therefore, no extrapolation for $N_b\to\infty$ can be attempted, and the asymptotic value of γ for bottle-brushes requires further

TABLE II. Exponents of the PDF for linear chains and LD bottle-brushes with $N_a=5$ beads per arm [see Eq. (12)]. The standard errors on the last significant digit are reported in parentheses.

	Linear		LD	
N_b	δ_0	ϑ_0	δ_0	ϑ_0
10	2.42(3)	0.38(4)	2.62(4)	0.64(4)
20	2.41(3)	0.38(3)	2.90(3)	0.91(3)
30			3.05(4)	0.93(4)
50	2.41(2)	0.32(2)	3.17(6)	0.80(5)
100	2.45(2)	0.26(2)	3.33(8)	0.41(6)

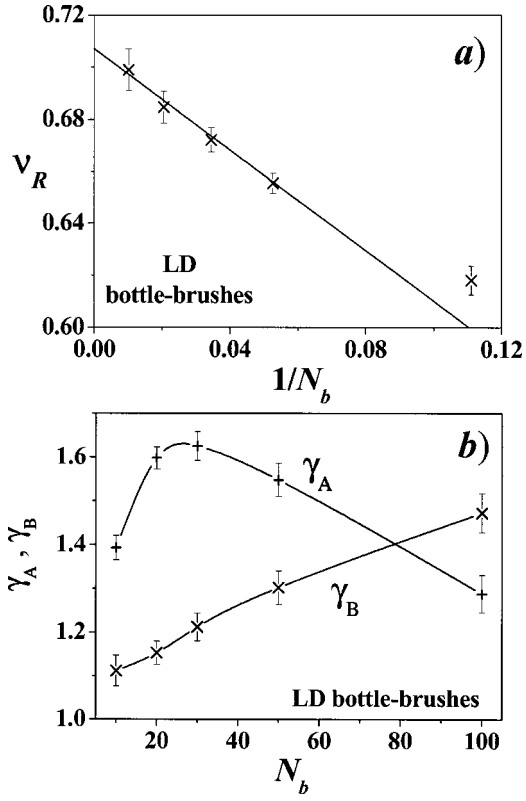

FIG. 6. (a) The Flory exponent ν_R extracted via Eq. (13) from the δ exponent obtained by fitting the PDF in Fig. 5, plotted vs N_b^{-1}. The values apply to LD bottle-brushes with $N_a=5$ beads per arm and were fitted neglecting the right-most data point. From linear extrapolation to $N_b^{-1}\to 0$, we obtain $\nu_R=0.706(7)$. (b) The critical exponent γ extracted via Eqs. (14) from the fitting ϑ_0 exponent of the PDF in Fig. 5 plotted vs N_b for the same bottle-brush as in panel (a). The solid curves are drawn as a guide for the eye.

study. We have also analyzed the PDF of the distances involving inner backbone beads in the LD bottle-brush with $N_b=100$ backbone beads and $N_a=5$ beads per arm. The data were again well fitted by Eq. (12), producing the exponents ϑ_1, δ_1 (end-to-center beads) and ϑ_2, δ_2 (center-to-center beads). The resulting values are $\vartheta_1=1.21(5)$ and $\vartheta_2=1.9(2)$, showing a pronounced widening of the correlation hole, with an upward curvature at small $\hat{r}$, unlike that found for the end-to-end beads. As for the δ exponents, we obtained $\delta_1=3.18(5)$ and $\delta_2=3.04(9)$, which are not significantly different and are both very close to δ_0 (see Table II), suggesting that they may attain a common value just as in linear chains.

Finally, we note that the ϑ_0 exponents of Table II imply that the detailed shapes of the PDF curves for linear chains and bottle-brushes reflect quantitative differences basically related to the width of the correlation hole at the origin, which depends both on the branching density and on the arms length. In fact, Fig. 7 shows that the maxima shift to larger distances upon increasing the arm length, with a wider correlation hole that would be even larger if we used r instead of $\hat{r}=r/\langle R_b^2\rangle^{1/2}$ due to the increase of $\langle R_b^2\rangle$ with increasing N_a. The shift of the maxima brings about also a peak sharpening, so that the distribution of the end-to-end distance becomes narrower, with smaller fluctuations around the average value. This feature is consistent with an apparent

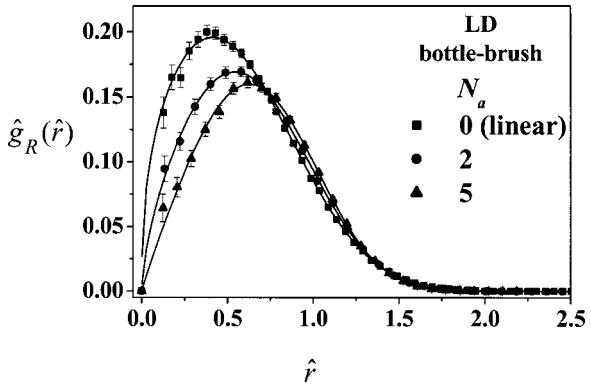

FIG. 7. The probability distribution function for the end-to-end distance R_b of a linear chain and two LD bottle-brushes with different arm lengths and a backbone with $N_b=20$ beads. The data were obtained with 1.0×10^5, 5.0×10^4, and 3.6×10^4 independent samples, from top to bottom, and the solid lines are the fitting curves obtained with Eq. (12).

backbone stiffening induced by the interactions among the side chains which increase with the arm length.

C. The backbone persistence length and the molecular aspect ratio

The average projection of the end-to-end vector $\mathbf{R}_b$ on the generic kth backbone spring yields the backbone persistence length $l_{\text{pers}}^{(k)}$ [see Eq. (5)]. This quantity is plotted vs k in Fig. 8 for linear chains and LD bottle-brushes of different length. Due to the greater freedom of the free ends, $l_{\text{pers}}^{(k)}$ is larger for inner springs, where it develops a well-defined plateau. The average plateau value defines the effective persistence length l_{pers}, which increases with the backbone length, whereas in ideal models it is a local property independent of molar mass. Thus, l_{pers} is affected by excluded-volume interactions among topologically distant beads, but it provides nonetheless a good measure of apparent stiffness. In Fig. 9, l_{pers} is plotted as a function of the number of backbone springs n_b for linear chains and LD and HD bottle-brushes at a fixed arm length showing the larger stiffness of bottle-brushes. Moreover, l_{pers} does increase with increasing

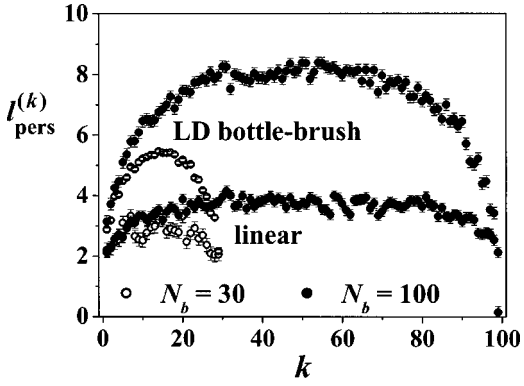

FIG. 8. The persistence length $l_{\text{pers}}^{(k)}$ obtained through Eq. (5) for the linear chain (lower data points) and the LD bottle-brushes with $N_a=5$ beads per arm (upper data points) as a function of the spring location k within the chain ($k=1$ and $k=N_b-1$ are the terminal spring) for different backbone lengths.

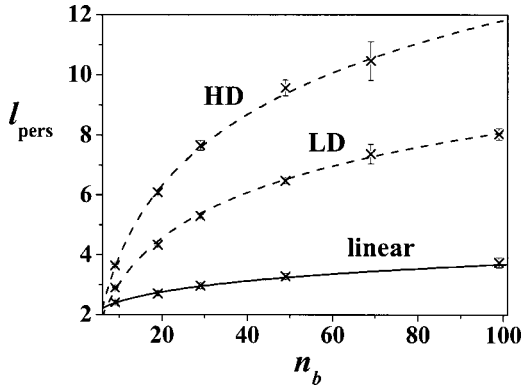

FIG. 9. The persistence length l_{pers}, given by the average plateau value of the data in Fig. 8, plotted as a function of the number of backbone springs n_b for linear chains and LD and HD bottle-brushes with $N_a=5$ beads per arm. The power-law fit for linear chains, according to Eq. (16), is shown with the solid curve. No satisfactory power law holds for the bottle-brushes, whose data points are smoothly connected by dashed lines as a guide for the eye.

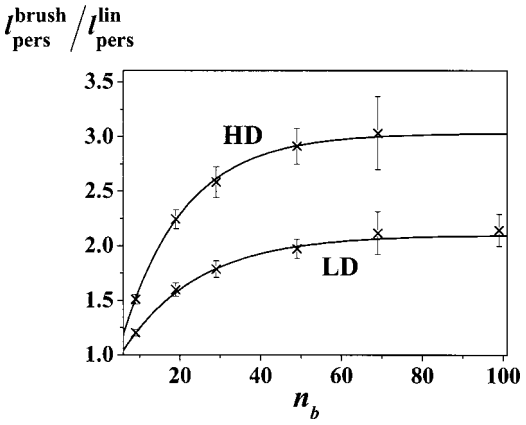

FIG. 10. The ratio $l_{pers}^{brush}/l_{pers}^{lin}$ plotted as a function of the number of backbone springs n_b for LD and HD bottle-brushes. The solid lines are the best-fit curves of Eq. (17) with $A=0.6(2)$, $B=1.5(1)$, $C=19(5)$ for LD, and $A=0.3(4)$, $B=2.7(3)$, $C=15(5)$ for HD bottle-brushes.

branching density m at a fixed arm length N_a (see Fig. 9), but also with increasing N_a at a fixed m and n_b to a constant value (results not shown).

Interestingly, for the linear chain, l_{pers} has a power-law dependence on n_b,

$$l_{pers}=a\cdot n_b^{\xi}, \tag{16}$$

where $a=1.61(8)$ and $\xi=0.18(1)$, confirming that it is indeed affected by excluded-volume interactions. In fact, considering that for linear chains with a contour length $L\gg l_{pers}$ we have $\langle R_b^2\rangle=2Ll_{pers}$, we obtain $\langle R_b^2\rangle=3.22(8)\cdot n_b^{1+\xi}$, where both the Flory exponent $\nu_R=(1+\xi)/2=0.59(1)$ and the prefactor agree with the parameters of Table I. On the other hand, no satisfactory power-law relationship holds for bottle-brushes, while for instance both an exponential saturation curve and a logarithmic-growth curve reasonably fit the data points, possibly showing crossover effects due to the limited range of N_b. However, if we normalize the bottle-brushes persistence lengths through the corresponding linear chain, the resulting ratio $l_{pers}^{brush}/l_{pers}^{lin}$ shows a saturation behavior (see Fig. 10). This ratio is larger than unity, indicating an increased stiffness due to the interarm repulsion, and is well reproduced by the functional form

$$l_{pers}^{brush}/l_{pers}^{lin}=A+B[1-\exp(-n_b/C)] \tag{17}$$

for both bottle-brushes. The very existence of a plateau for this ratio indicates that the effect of the good-solvent expansion on l_{pers} is asymptotically the same in linear chains and in bottle-brushes. In turn, this behavior suggests that the additional backbone stiffening in bottle-brushes compared to linear chains is basically local, and accordingly, the same asymptotic behavior and Flory exponent should eventually be attained.

We additionally report in Fig. 11 the aspect ratio, defined as l_{pers}/D, where D is the molecular diameter, taken as twice the average root-mean-square end-to-end distance of the arms, i.e., $D=2\langle R_a^2\rangle^{1/2}$. Because of the uniform value of $\langle R_a^2\rangle$ mentioned before, and hence of D, the aspect ratio steadily increases with increasing backbone length at a fixed arm size similar to the increase of l_{pers} in Fig. 9, possibly to an asymptotic constant value. The aspect ratio is larger at larger branching density, but it barely exceeds unity. Recent simulations[12] reported a persistence length strongly increasing with the arm length, but with an aspect ratio l_{pers}/D that was constant for flexible side chains, and sharply increasing for stiff arms. It should be remembered here that when the aspect ratio exceeds a value of 10 in a semiflexible chain, lyotropic behavior is predicted.[6,27,28] Clearly, no such behavior is expected with the present simulation parameters.

In this context, however, it should be pointed out that the definition of l_{pers} is by no means unique, and different definitions or different ways of calculating it from simulation results may lead to rather different values. For instance, ten Brinke *et al.*[12] initially attempted to estimate l_{pers} by fitting the calculated radius of gyration to the wormlike expression, thus obtaining values quite similar to ours. However, they also obtained a different value from the plots of the correlation function $\langle\cos\vartheta_{ij}\rangle$ of the bond angles formed by the backbone segments as a function of their topological separation. Under the simplifying assumption of a simple exponential decay, at least for not-too-close segments, this procedure

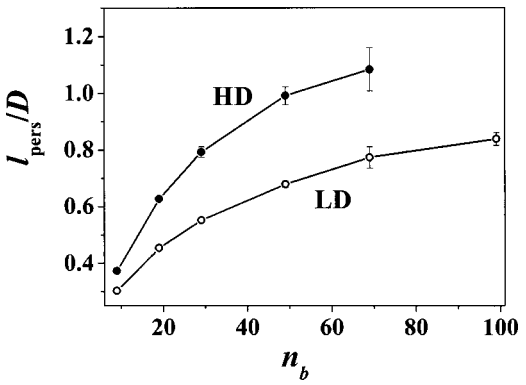

FIG. 11. The molecular aspect ratio l_{pers}/D, D being the molecular diameter, plotted as a function of the number of backbone springs n_b for the LD and HD bottle-brushes at a fixed arm length $N_a=5$. The solid lines are drawn as a guide for the eye.

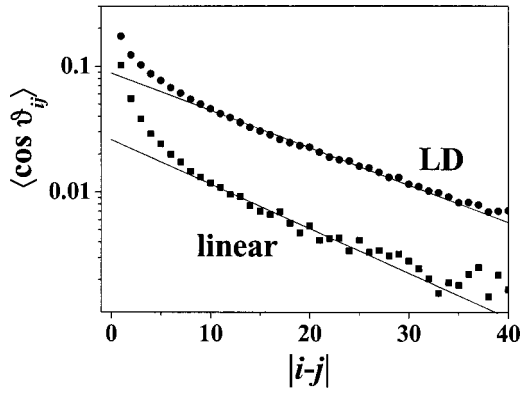

FIG. 12. The average cosine of the angle between the i,j backbone springs plotted as a function of their topological separation mediated over all the positions of the first spring according to Eq. (18) for the linear chain (bottom data) and for the LD bottle-brush with $N_a=5$ (in both cases, $N_b=100$). The solid lines are the best fits obtained with a simple exponential in the range $10<|i-j|<30$ for the linear chain, and $10<|i-j|<40$ for the LD bottle-brush.

yielded much larger values of l_{pers}. Accordingly, we adopted the same procedure, and calculated the same correlation function, averaged over all the possible positions along the backbone, through the expression

$$\langle \cos \vartheta_{ij} \rangle = \frac{1}{n_b - |i-j|} \sum_{i=1}^{n_b-|i-j|} \langle \mathbf{u}_i \cdot \mathbf{u}_j \rangle, \tag{18}$$

where $\mathbf{u}_i = \mathbf{r}_i / |\mathbf{r}_i|$ is the unit vector associated with the ith spring. The plot of $\langle \cos \vartheta_{ij} \rangle$ versus $|i-j|$ is reported in Fig. 12 for a linear chain and an LD bottle-brush. Following ten Brinke *et al.*,[12] we fitted the linear portion of the semilogarithmic plot to a simple exponential, $\exp(-|i-j|/l_{\text{pers}})$, thus obtaining a different estimate of l_{pers}. The best-fit lines, shown on the plots, yielded $l_{\text{pers}}=12.2(4)$ for the linear chain, and 14.6(2) for the LD bottle-brush. Though clearly dependent both on the assumed exponential decay and on the fitting range, both values are much larger than those previously obtained, and in full agreement with previous results.[12] We finally mention that we are presently carrying out new simulations of LD bottle-brushes with the arm beads having a diameter twice as large as the backbone beads. Preliminary results indicate larger persistence lengths, equal to 14.5(3) using our former procedure or to 17.4(1) using the latter one. It is thus possible that by modifying the microscopic model, for instance by introducing an intrinsic backbone stiffness and/or increasing the bead diameters we may reproduce the observed lyotropic behavior of bottle-brushes.[3,4]

D. The static structure factor

We finally turn to the static structure factor $S(q)$. Note that, experimentally, if the side chains do not provide any contrast with the solvent, one can measure the backbone scattering only, $S_b(q)$. Hence, we report this quantity in Fig. 13(a) for a linear chain and LD and HD bottle-brushes with $N_a=5$ beads per arm, as a function of q in a double logarithmic plot. At large q, we expect $S_b(q)$ to scale as $S_b(q) \propto q^{-1/\nu}$, as indeed manifested by the best-fit lines, providing an additional estimate of the ν exponent. The resulting values

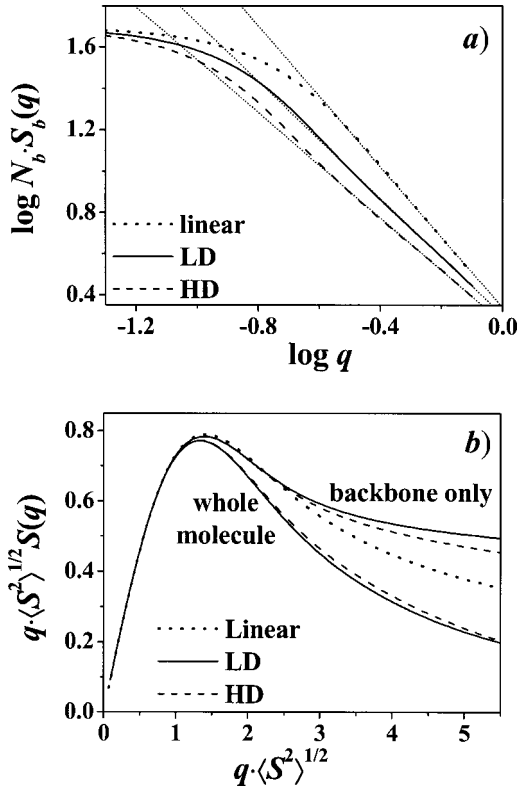

FIG. 13. (a) The static structure factor due to the backbone only plotted as $N_b \cdot S_b(q)$ vs q in double logarithmic scales for the linear chain (dotted curve), and the LD and HD bottle-brushes (solid and dashed curves) with $N_a=5$ beads per arm and a backbone with $N_b=50$ beads. The thin dotted lines are the best fits to the power law $S_b(q) \propto q^{-1/\nu}$. (b) The static structure factor for the linear chain and the LD and HD bottle-brushes plotted as $q\langle S^2 \rangle^{1/2} S(q)$ as a function of $q\langle S^2 \rangle^{1/2}$. The two curves below the dotted curve of the linear chain show the structure factor of the whole bottle-brushes (all beads are scattering centers), and the two curves above it the structure factor of the backbone only (the arms do not give any contrast with the solvent), $\langle S^2 \rangle^{1/2}$ being here $\langle S_b^2 \rangle^{1/2}$.

are 0.5872(2) for the linear chain, 0.7067(3) for the LD and 0.786(1) for the HD bottle-brush. Such values well agree with those reported in Table I or extrapolated from Fig. 6, being only slightly larger for the HD bottle-brush.

A different display of the static structure factor is shown in Fig. 13(b), where we plot $q\langle S^2 \rangle^{1/2} S(q)$ as a function of $q\langle S^2 \rangle^{1/2}$ considering both the whole molecule and the backbone only. For the whole molecule, the LD and HD bottle-brushes display a sharper peak than the corresponding linear chain simply due to the increased concentration of monomers near the branch points, with only a minor difference between the two bottle-brushes in spite of the different branching density. Conversely, the structure factor of the bottle-brushes backbone, $S_b(q)$, is larger than for the corresponding linear chain, owing to the greater expansion and to the backbone stiffening. In this case, some difference between the two bottle-brushes is apparent. The format of Fig. 13(b) was chosen because at large q such that $q \cdot l_{\text{pers}} > 1$, stiff chains should display a rodlike behavior, with $S(q)$ proportional to q^{-1}, so that $q \cdot S(q)$ should decrease to a constant value. No such behavior is obtained from our simulations down to the shortest observation distance, roughly corresponding to the average spring length. This result is consis-

tent with the relatively small persistence length previously discussed, and indicates once more that, with the present parameters, our bottle-brushes do not follow the wormlike-chain behavior. On the other hand, such behavior for the bottle-brush backbone has been experimentally observed by neutron scattering in a poly(chlorovinyl ether) grafted with polystyrene using matching conditions for the side chains.[29] While our bottle-brushes are probably too short for a direct comparison, we believe that our choice of the same bead diameter for the backbone and for the arms, as well as the lack of any intrinsic backbone stiffness yields a larger flexibility than observed in Ref. 29.

IV. CONCLUDING REMARKS

In this paper we report the results of a continuous space Monte Carlo simulation of molecular bottle-brushes adopting a bead-and-spring model with a hard-sphere potential to account for excluded-volume interactions. We are thus in the athermal regime of a pure self-avoiding walk with topological connectivity constraints. We first focus on the global properties such as the backbone mean-square end-to-end distance and radius of gyration, and interbead distances, and then on the probability distribution functions of the distances among the beads, on the apparent persistence length of the backbone, and, finally, on the static structure factor. We find that the molecular size shows a power-law dependence on the backbone length with a swelling exponent much larger than in linear chains. This feature is attributed to the interarm repulsions due to the large density of branching, that can be relieved somewhat by an apparent backbone stiffening. An independent estimate of the swelling exponents extracted from the probability distribution functions for the backbone end-to-end distance is fully consistent with the results obtained from the power-law fit, as does the estimate obtained from the static structure factor at large scattering vector.

On the other hand, we have some evidence suggesting that these results may still be in a crossover region, while the asymptotic behavior would be reached only for huge backbone lengths. Some evidence of such crossover comes from the plots of the backbone persistence length l_{pers} of bottle-brushes, which is larger than in linear chains due to the stiffening induced by the interarm repulsions. However, l_{pers} asymptotically increases with the backbone length in the same way as in linear chains, and therefore it eventually becomes independent of topology, apart from a trivial scale factor [here we refer to the model-independent definition of persistence length given in Eq. (5)]. Therefore, the same behavior should eventually be shown by linear chains and comb polymers, although bottle-brushes would achieve the asymptotic behavior only for huge sizes, possibly outside the experimental range. From the theoretical viewpoint, this is still an unsolved and complicated issue, since it requires establishing the critical exponent for the backbone size at a finite arm length.

We also determined the probability distribution function for the backbone end-to-end distance and estimated the critical exponents of bottle-brushes. We also showed that in these systems the correlation hole widens with the length of the side chains, a feature consistent with the backbone stiffening. On the other hand, the static structure factor of the backbone $S_b(q)$ does not become proportional to q^{-1}, q being the momentum transfer, unlike what expected at large q for stiff chains and what has been observed experimentally by neutron scattering. Moreover, the backbone stiffening with a constant molecular diameter at a fixed arm length increases the molecular aspect ratio, which however is not large enough as to suggest a lyotropic behavior, unlike what is found experimentally in some cases, possibly due also to packing effects. On the other hand, by changing the model parameters such as the bead diameter ratio for the backbone and the side chains, as well as by adding an intrinsic bending potential, we can achieve a further stiffening of the backbone. We hope to address these issues in a future work.

ACKNOWLEDGMENTS

This paper is dedicated to Professor Giuseppe Allegra. The authors gratefully thank Professor Giuseppe Allegra for useful discussions, and Enterprise Ireland for travel Grants Nos. IC/2003/037 and IC/1999/001. This work was financially supported by the Italian Ministry for Instruction, University and Research.

[1] M. Wintermantel, M. Gerle, K. Fischer, M. Schmidt, I. Wataoka, H. Urakawa, K. Kajiwara, and Y. Tsukahara, Macromolecules **29**, 978 (1996).
[2] Y. Tsukahara, K. Mizuno, A. Segawa, and Y. Yamashita, Macromolecules **22**, 1546 (1989); Y. Tsukahara, K. Tsutsumi, Y. Yamashita, and S. Shimada, *ibid.* **23**, 5201 (1990).
[3] M. Wintermantel, K. Fischer, M. Gerle, R. Ries, M. Schmidt, K. Kajiwara, H. Urakawa, and I. Wataoka, Angew. Chem., Int. Ed. Engl. **34**, 1472 (1995).
[4] P. Dziezok, S. S. Sheiko, K. Fischer, M. Schmidt, and M. Möller, Angew. Chem., Int. Ed. Engl. **36**, 2812 (1997).
[5] R. Djalali, S.-Y. Li, and M. Schmidt, Macromolecules **35**, 4282 (2002).
[6] M. Saariaho, O. Ikkala, I. Szleifer, I. Erukhimovich, and G. ten Brinke, J. Chem. Phys. **107**, 3267 (1997).
[7] M. Saariaho, I. Szleifer, O. Ikkala, and G. ten Brinke, Macromol. Theory Simul. **7**, 211 (1998).
[8] R. Djalali, N. Hugenberg, K. Fischer, and M. Schmidt, Macromol. Rapid Commun. **20**, 444 (1999).
[9] J. Ruokolainen, G. ten Brinke, O. Ikkala, M. Torkkeli, and R. Serimaa, Macromolecules **29**, 3409 (1996).
[10] K. Shiokawa, K. Itoh, and N. Nemoto, J. Chem. Phys. **111**, 8165 (1999).
[11] P. G. Khalatur, D. G. Shirvanyanz, N. Yu. Starovoitova, and A. R. Khokhlov, Macromol. Theory Simul. **9**, 141 (2000).
[12] M. Saariaho, A. Subbotin, I. Szleifer, O. Ikkala, and G. ten Brinke, Macromolecules **32**, 4439 (1999); M. Saariaho, O. Ikkala, and G. ten Brinke, J. Chem. Phys. **110**, 1180 (1999); M. Saariaho, A. Subbotin, O. Ikkala, and G. ten Brinke, Macromol. Rapid Commun. **21**, 110 (2000).
[13] G. H. Fredrickson, Macromolecules **26**, 2825 (1993); A. Subbotin, M. Saariaho, O. Ikkala, and G. ten Brinke, *ibid.* **33**, 3447 (2000).
[14] T. M. Birshtein, O. V. Borisov, Y. B. Zhulina, A. R. Khokhlov, and T. A. Yurasova, Polym. Sci. U.S.S.R. **29**, 1293 (1987).
[15] F. Ganazzoli, Yu. A. Kuznetsov, and E. G. Timoshenko, Macromol. Theory Simul. **10**, 325 (2001).
[16] F. Ganazzoli, R. La Ferla, and G. Raffaini, Macromolecules **34**, 4222 (2001); F. Ganazzoli, R. La Ferla, and G. Terragni, *ibid.* **33**, 6611 (2000); F. Ganazzoli, Condens. Matter Phys. **5**, 37 (2002).
[17] E. G. Timoshenko, Yu. A. Kuznetsov, and R. Connolly, J. Chem. Phys. **117**, 9050 (2002); **116**, 3905 (2002).
[18] R. Connolly, E. G. Timoshenko, and Yu. A. Kuznetsov, J. Chem. Phys. **119**, 8736 (2003).
[19] M. P. Allen and D. J. Tildeslay, *Computer Simulation of Liquids* (Oxford University Press, Oxford, 1987).
[20] P. J. Flory, *Statistical Mechanics of Chain Molecules* (Wiley Interscience, New York, 1969).

[21] R. Guida and J. Zinn-Justin, J. Phys. A **31**, 8103 (1998).
[22] C. Domb, J. Gillis, and G. Wilmers, Proc. Phys. Soc. London **85**, 625 (1965).
[23] M. E. Fisher, J. Chem. Phys. **44**, 616 (1966); D. S. McKenzie and M. A. Moore, J. Phys. A **4**, L82 (1971).
[24] J. des Cloizeaux, Phys. Rev. A **10**, 1665 (1974); J. Phys. **41**, 223 (1980).
[25] B. Duplantier, J. Stat. Phys. **54**, 581 (1989).
[26] S. Müller and L. Schäfer, Eur. Phys. J.: Appl. Phys. **2**, 351 (1998).
[27] L. Onsager, Ann. N.Y. Acad. Sci. **51**, 627 (1949).
[28] A. Khokhlov and A. N. Semenov, Physica A **108**, 546 (1981).
[29] S. Lecommandoux, F. Chécot, R. Borsali, M. Schappacher, A. Deffieux, A. Brûlet, and J. P. Cotton, Macromolecules **35**, 8878 (2002).